

Article

Green Synthesis of De Novo Bioinspired Porous Iron-Tannate Microstructures with Amphoteric Surface Properties

Hemali Rathnayake *, Sheeba Dawood, Gayani Pathiraja , Kelvin Adrah and Olubunmi Ayodele 

Nanoscience/Joint School of Nanoscience and Nanoengineering, University of North Carolina at Greensboro, Greensboro, NC 27401, USA; sheebadawood@gmail.com (S.D.); gcpathir@uncg.edu (G.P.); k_adrah@uncg.edu (K.A.); ooayodel@uncg.edu (O.A.)

* Correspondence: hprathna@uncg.edu; Tel.: +1-336-285-2860

Abstract: Bioinspired porous microstructures of iron-tannate (Fe(III)-TA) coordination polymer framework were synthesized by catenating natural tannic acid with iron(II), using a scalable aqueous synthesis method in ambient conditions. The chemical composition, morphology, physiochemical properties, and colloidal stability of microstructures were elucidated. The surface area (S_{BET}) and the desorption pore volume were measured to be $70.47 \text{ m}^2/\text{g}$ and $0.44 \text{ cm}^3/\text{g}$, respectively, and the porous structure was confirmed with an average pore dimension of $\sim 27 \text{ nm}$. Microstructures were thermally stable up to $180 \text{ }^\circ\text{C}$, with an initial weight loss of 13.7% at $180 \text{ }^\circ\text{C}$. They exhibited high chemical stability with pH-responsive amphoteric properties in aqueous media at pH levels ranging from 2 to 12. Supporting their amphoteric sorption, microstructures exhibited rapid removal of Pb^{+2} from water, with 99% removal efficiency, yielding a maximum sorption capacity of 166.66 mg/g . Amphoteric microstructures of bioinspired metal-phenolate coordination polymers remain largely unexplored. Additionally, natural polyphenols have seldomly been used as polytopic linkers to construct both porous and pH-responsive amphoteric coordination polymer frameworks with a robust structure in both acidic and basic media. Thus, this de novo porous microstructure of Fe(III)-TA and its physiochemical surface properties have opened new avenues to design thermally and chemically stable, eco-friendly, low-cost amphoteric sorbents with multifunctionality for adsorption, ion exchange, separation, storage, and sensing of both anions and cations present in heterogeneous media.

Keywords: green synthesis; amphoteric surface properties; biopolymers; natural polyphenols; tannic acid



Citation: Rathnayake, H.; Dawood, S.; Pathiraja, G.; Adrah, K.; Ayodele, O. Green Synthesis of De Novo Bioinspired Porous Iron-Tannate Microstructures with Amphoteric Surface Properties. *Sustain. Chem.* **2022**, *3*, 192–204. <https://doi.org/10.3390/suschem3020013>

Academic Editors: Francesca Deganello, Maria Luisa Testa and Sergio Gonzalez-Cortes

Received: 28 February 2022

Accepted: 18 April 2022

Published: 5 May 2022

Publisher's Note: MDPI stays neutral with regard to jurisdictional claims in published maps and institutional affiliations.



Copyright: © 2022 by the authors. Licensee MDPI, Basel, Switzerland. This article is an open access article distributed under the terms and conditions of the Creative Commons Attribution (CC BY) license (<https://creativecommons.org/licenses/by/4.0/>).

1. Introduction

Bioinspired metal-organic coordination polymers with outstanding physiochemical properties are expected to be of intense interest in the development of advanced multifunctional hybrid materials—for example, environmentally benign hybrid materials with amphoteric natures that display cationic behavior below the isoelectric point and anionic behavior at higher pH and offer unique properties, such as high surface activities and selectivity for analytes, a wide isoelectric range, bioactivity, and high interface interactions [1]. Because of these physiochemical properties, amphoteric materials have been attractive as mixed-mode ion-exchange sorbents in the fields of cosmetics, chromatography, oil recovery, electrochemistry, nanoscience, polymer chemistry, and wastewater treatment [1,2]. Specifically, amphoteric sorbents are intended to enhance the sensitivity and selectivity of solid-phase, extraction-based methods, thereby enabling increasingly complex matrixes to be handled. These sorbents are either silica-based or organic polymer-based, with the ion selectivity arising from the presence of ionizable functional groups able to interact with anionic and cationic species [3,4]. To date, however, no bio-based amphoteric porous microstructures with robust coordination polymer frameworks have been developed from low-cost, readily available biomass precursors or biopolymers.

Considering the potential stability of metal–phenolate coordination bonds—together with the growing global demand to broaden the use of renewable resources—synthesis of natural polyphenol-based sorbents with amphoteric characteristics has appeal for the solid-phase extraction of acidic and basic analytes [5,6]. They have the ability to act as multifunctional rigid spacers between cations, contributing to the porosity of the resulting coordination polymer framework, with additional functionalities, such as phenolic, carbonyls, esters, and cyclic ether groups. Therefore, they show great promise as a rich supply of precursors for green chemistry and strong ion exchangers that could charge across the entire pH range of operation, providing opportunities for the development of bioinspired sorbents for environmental remediation.

Coordination polymers (CPs) and their subclass, metal–organic frameworks (MOFs) are highly porous self-assembled nanostructures with high surface areas and defined pore dimensions. They have been used in a wide range of applications, such as gas storage and separation, drug delivery and storage, chemical separation, sensing, catalysis, and bio-imaging [7]. The MOFs precisely position metal-based nodes by connecting them with functional organic ligands via coordination bonds. Compared with traditional porous solids, such as zeolites, activated carbon and mesoporous silica, MOFs allow for designed framework structures and tailored pore environments at the molecular level. Their size, shape, and self-assembly can be carefully controlled via an effective covalent synthesis method to yield three-dimensional (3-D) hierarchical architectures. They offer a new method for fine-tuning structural nodes with known geometries and coordination environments. Their porous structures and the geometric arrangement of inorganic and organic components enable rational design for high surface area platforms [8]. Exploring the potential design and synthesis of naturally abundant and environmentally friendly novel classes of coordination polymer frameworks similar to MOFs' robust metal–carboxylate framework, herein, for the first time, we developed a *de novo* bio-based coordination polymer framework with amphoteric properties by coordinating Fe^{+3} metal nodes with a highly branched polytopic organic ligand (tannic acid) to yield a porous and robust structure of iron-tannate coordination polymer framework (Fe(II)-TA). Its amphoteric properties were revealed for the first time, and its potential applicability for heavy metal adsorption from water was demonstrated.

Tannic acid (TA) is a natural polyphenol and one of the cheapest natural abundant functional materials [9,10]. Its five pyrogallol and five catechol groups provide multiple bonding sites with diverse interactions, such as ionic, coordination, hydrogen bonding, and hydrophobic interactions [11–13]. Its oxygen-rich functional groups, which include catechol and pyrogallol groups, can coordinate with variety of transition metal ions, forming coordination complexes. They possess metal–phenolic coordination and have been explored in the past [14–18]. A variety of metal–tannate coordination complexes and polymers have been applied as either thin films or particles with tailored properties [14] or in the formation of novel metallogels [17]. The use of TA as either porogen or an additive component in materials science has attracted great attention. This is due not only to its cheap, environmentally friendly, and nontoxic nature, but also its ability to be used as a non-surfactant template. For example, past research has demonstrated that TA can be used as a porogen to tune the porosity of other inorganic particles and make mesoporous materials with tunable mesopore sizes ranging from 6 to 13 nm [19–23]. The coordination complex formation between tannic acid and iron(III) was demonstrated recently, albeit in a very few literature reports [24–28]. A supramolecular assembly of iron(III)-tannic acid metal–organic complex was developed as an antimicrobial spray nanocoating. It has demonstrated its utility as an antimicrobial coating in shoe insoles and fruits [24]. Additionally, a molecular nanoparticle-based Fe(III)-tannic acid complex was previously synthesized using a low-cost, reproducible method and its physicochemical properties (including its capability of inducing autophagy effect in two selected liver cell lines) were studied [25–28]. Furthermore, a self-assembly of metal ions with tannic acid on various

substrates was demonstrated using coordination programming to prepare multifunctional thin films and capsules [29–33].

Despite the aforementioned research advances in bio-based metal–tannic acid coordination materials, very few studies have reported using iron–tannate coordination complexes either as an adsorbent or an adsorptive catalyst for removing the fluorides, organic dyes, and nitrogen compounds present in water resources [34–36]. In all these prior studies, metal–tannate was a catenated organometallic complex with no robust coordination framework where the metal nodes precisely coordinated onto the catechol units to make a robust metal–phenolate coordination geometry that controlled the porosity of hierarchical microstructures of Fe(III)-TA coordination polymer frameworks. Thus, our microstructure of Fe(III)-TA coordination polymer frameworks was *de novo* and possessed porous hierarchical coordination geometry with a robust structural framework similar to MOFs architectures, but constructed from a polytopic organic ligand and metal nodes [7,8]. Additionally, the porous microstructures of iron–tannate coordination polymer frameworks with tailored amphoteric surface properties were not reported, nor were their potential applicability as sorbents to remove heavy metals from water demonstrated. Thus, the work described herein contributed to the first synthesis of a *de novo* bioinspired sorbent with amphoteric properties.

2. Materials and Methods

2.1. Materials

Tannic acid ($C_{76}H_{52}O_{46}$, Molar Mass = $1701.19 \text{ g mol}^{-1}$), iron(II) acetate hexahydrate, and anhydrous ethanol were obtained from Sigma-Aldrich (St Louis, MO, USA). Unless otherwise stated, all chemicals were used as received.

2.2. Procedure for the Preparation of Fe(III)-TA Microstructures

The self-assembled microstructures were prepared at room temperature by dissolving 1:10 molar ratio of tannic acid (0.10 g, 0.05 mmol) to iron(II) acetate (0.10 g, 0.50 mmol) in DI water (each 10 mL in volume). Initial pH of both solutions were recorded. The initial pH of the tannic acid and Fe^{+2} solutions were 3.28 and 5.51, respectively. The iron(II) acetate solution was added into the tannic acid solution in a 50 mL beaker dropwise (0.5 mL/min) with rapid stirring at room temperature. Initially, light purple (Lilac color,) precipitate was formed; gradually, it turned dark purple on complete addition of Fe^{+2} solution. The nanostructure formation was monitored using UV-visible spectroscopy by taking an aliquot from the reaction mixture just after the addition of the ion solution after stirring for one hour. The darker purple suspension that resulted was imaged under TEM. The suspension was transferred into a 50 mL falcon tube and sonicated for one additional hour to break any aggregation. After sonication, 1 mL of sample was taken for morphology analysis using TEM, SEM, and UV-vis. The dark purple precipitate was collected by centrifugation at 10,000 RPM for 10 min. The sample was dried under vacuum at -25 Torr at room temperature to yield dark purple powder (80% yield). The structural composition was analyzed by FT-IR and micro-elemental analysis and oxidation states of each element were confirmed by elemental analyzer and XPS, respectively. FT-IR stretching (cm^{-1}): 3421 (broad peak, $-OH$), 1689 (sharp peak, metal ion-coordinated carbonyls in pyrogallol units), 1608–1446 (weak multiple peaks, $C=C$ aromatic), 1330 (sharp peak, $C-O-C=O$), 1106, and 1036 (sharp peaks, $C-O-C$); elemental composition by XPS: C (45.33%), Fe (11.62%), and O (39.05%); micro-elemental analysis (experimental): C (45.79%), and H (3.19); calculated for empirical formula of $Fe_4C_{72}H_{40}O_{46}-C$ (46.38%), Fe (11.98%), H (2.16%), and O (39.47%).

2.3. Characterization

The chemical composition and functional groups were analyzed using Fourier transform infrared spectroscopy (FTIR-Varian 670-IR spectrometer, Agilent Technologies, Santa Clara, CA, USA). The morphology of the microstructures was analyzed using transmission electron microscopy (TEM Carl Zeiss Libra 120 and HR-TEM JEOL2100PLUS with STEM/EDS

capability at 120 kV and 200 kV, respectively) and scanning electron microscopy (Carl Zeiss Auriga FIB-FESEM, Carl Zeiss, Jena, Germany). Bulk elemental analysis was also obtained using energy dispersive X-ray spectroscopy (EDS) from JEOL IT800 SEM/EDS. The thermal stability of the microstructures was analyzed using the thermogravimetric analyzer (Q500). Samples were heated up to 700 °C at increments of 10 °C/min in nitrogen gas flow. The elemental compositions for C and H were obtained from the micro-elemental analyzer. Chemical oxidation states of each element were obtained from X-ray photon spectroscopy (XPS-Escalab Xi+-Thermo Scientific, Thermo Fisher Scientific, Waltham, MA, USA). Elemental compositions for Fe, C, O were also obtained from XPS elemental survey analysis. Full N₂-isotherm with micropore analysis (Physi-13) for single point BET, BET surface area, micropore volume area using t-plot, and micropore volume distribution using DFT were conducted using Micromeritics 3Flex Gas Analyzer by Micromeritics Instrument Corp (Norcross, GA, USA). The sample was degassed under vacuum at 180 °C for 12 h, prior to collection of the N₂-isotherms. The Zeta potential of the microstructures was measured using the Zeta sizer dip cell kit (Malvern Nano ZS, Horiba, London, UK). Zeta potential measurements: microstructures (0.050 g) were dispersed in ethanol (99.5%) and DI water, respectively, and ultrasonicated for 15 min to get a colloidal suspension. The natural pH of sorbents was measured to be 6.22 in ethanol and 3.8 in water. The zeta potential measurements were performed for six different pH solutions (pH = 2, 4, 6, 7, 10 and 12) in ethanol and water at 20 °C using the Zeta sizer dip cell kit (Malvern Nano ZS, UK). The pH of each solution was adjusted by dropwise addition of appropriate amounts of 0.1 M NaOH or 0.1 M HCl. Three measurements of zeta potentials were taken for one sample and the median was recorded. The level of lead(II) ions in aqueous solutions, before and after being soaked with Fe(III)-TA sorbents, was analyzed using a simultaneous inductively coupled plasma optical emission spectrometer (ICP-OES) with trace element analysis capability for wavelengths from 177 to 785 nm (Varian 710-ES ICP Spectrophotometer, Agilent Technologies, Santa Clara, CA, USA) in 3% (v/v) nitric acid solution.

2.4. Lead (Pb²⁺) Adsorption Experiments

The Pb²⁺ ions adsorption was studied using a series of experiments at varied initial heavy metal ion concentrations ranging from 20 to 500 mg/L. In each test, the microstructures (20.0 mg) were dispersed and soaked in 10 mL of heavy metal ion solutions for 15 min to reach equilibrium. The initial and equilibrium pH were 5.88 and 3.72, respectively. The suspensions were filtered through 0.45 µm membrane filters and analyzed for heavy metal ion concentration using an ICP-OES in 2.5% (v/v) nitric acid solution. The amount of heavy metal ions adsorbed onto the sorbent at equilibrium (q_e) was calculated by mass balance equation of heavy metal ions before and after the sorption, using Equation (1):

$$q_e = \frac{(C_i - C_t)V}{W} \quad (1)$$

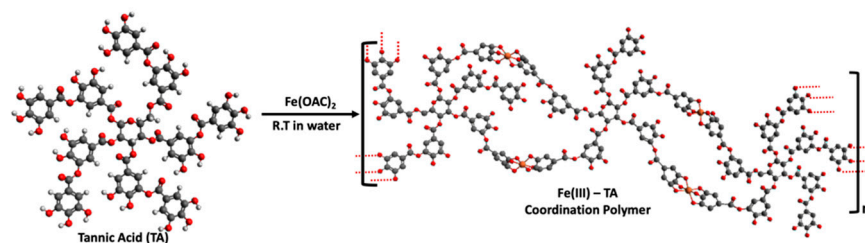
where q_e is the equilibrium sorption capacity, and C_i and C_t are initial and final heavy metal concentration, respectively, at equilibrium.

3. Results

3.1. Synthesis

The chemistry for the formation of Fe(III)-TA coordination polymers with hexacoordinated Fe(III)-phenolate coordination framework is depicted in Scheme 1. As described in the experimental procedure for the preparation of iron-tannate microstructures, our synthesis followed green chemistry principles. We utilized a renewable feedstock, a natural polyphenol as the precursor, water as the solvent, preventing toxic and hazardous chemicals, and room temperature chemical synthesis, providing an energy efficient synthesis approach, to produce bio-based Fe(III)-TA sorbent. In our synthesis, dropwise slow addition of aqueous solution of Fe²⁺ at a rate of 0.5 mL/min into the tannic acid aqueous solution while the reaction was stirring at room temperature yielded a lilac-colored pre-

precipitate which gradually turned to dark purple upon complete addition of iron acetate solution (Figure 1a,b). The gradual color change from the initial yellow color to purple and eventually dark purple during and after the addition of Fe^{+2} demonstrated that the complex formation was very rapid. Product formation was successful within an hour (Figure 1a,b). The final pH of the reaction mixture was 4.99.



Scheme 1. Synthesis scheme for the formation of Fe(III)-TA by catenating tannic acid with Fe^{+2} .

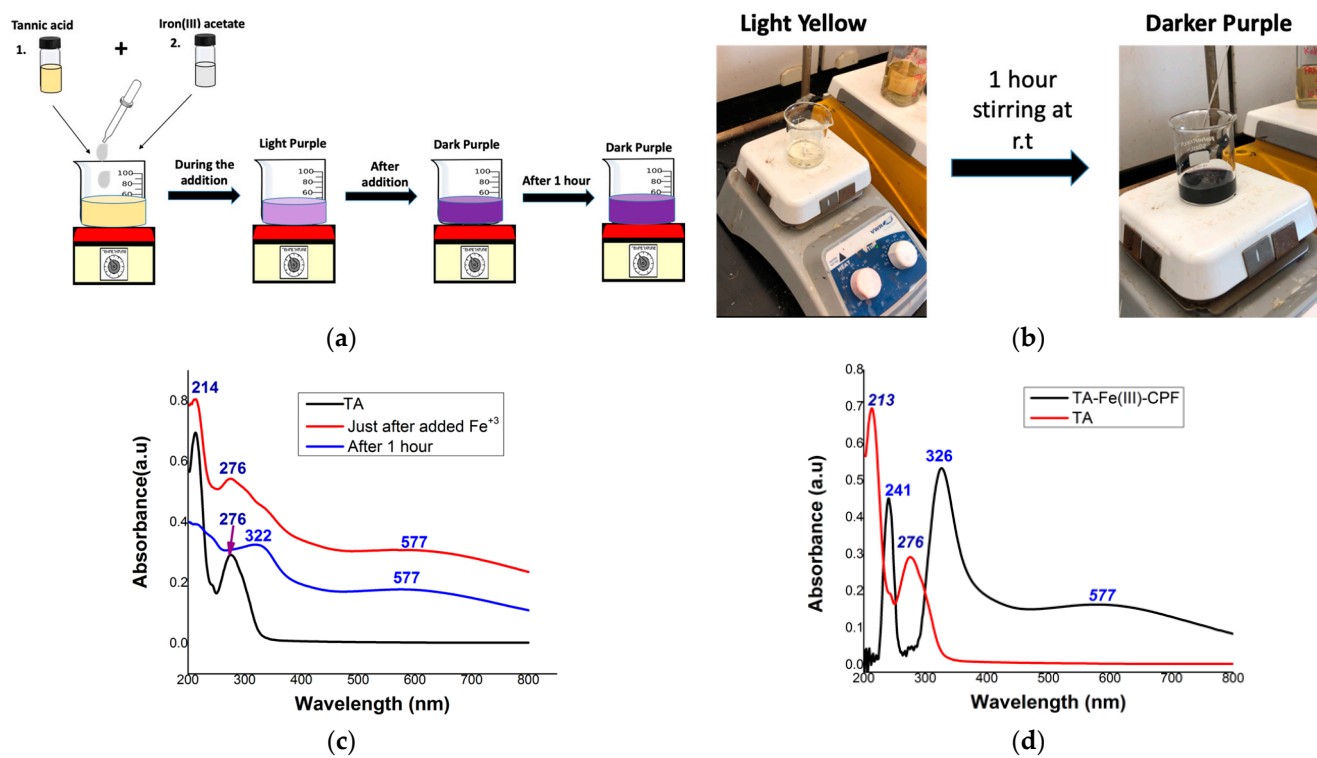


Figure 1. (a) Color changes during the reaction progress. (b) Images taken before addition of Fe^{+3} solution and after 1 h of reaction time. (c) Respective UV-visible spectral traces collected during the reaction progress. (d) A comparison of UV-visible spectra of tannic acid (TA) and purified and redispersed Fe(III)-TA microstructures in ethanol.

The product formation was monitored by collecting UV-visible spectra at the initial stage, during the reaction, and after one hour of reaction time, and comparing them with the UV-visible spectra taken for washed and purified nanoparticles after redispersal in ethanol (Figure 1c,d). The UV-visible spectrum of TA typically exhibited two absorption vibronic peaks at 214 nm and 276 nm, which corresponded to outer gallic acid units (catechol) and inner gallic acid units bonded to glucose moiety (pyrogallols), respectively. With the addition of Fe^{+2} solution, two characteristic vibrational peaks corresponding to TA showed a gradual red shift, to 241 nm and 326 nm, with an additional broader peak at 577 nm, demonstrating the formation of an oxidized Fe(III)-TA coordination framework. The broader peak at 577 nm corresponded to the charge transfer (CT) band, arising due

to complex formations between Fe(III) and TA and confirming the coordination bonding between Fe(III) and hydroxy groups of gallic acids [25].

3.2. Characterization

As depicted in Figure 2a, the FT-IR spectra confirmed the formation of Fe-O bonds from the presence of $\nu_{(\text{Fe-O})}$ stretch at 660 cm^{-1} and the shift of ester carbonyl of the catechol units, $\nu_{(\text{C=O})}$ from 1720 cm^{-1} to 1693 cm^{-1} . The chemical composition and monomer empirical formulae of Fe(III)-TA were deduced by combining surface analysis data obtained from the XPS elemental survey and micro-elemental analysis, supporting the presence of Fe, C, H, and O with the empirical formula $\text{Fe}_4\text{C}_{72}\text{H}_{40}\text{O}_{46}$. Since iron composition was obtained from the XPS elemental survey, a surface analysis method, EDS analysis (Figure S1) on the bulk sample was also performed to support the iron content present in Fe-TA microstructures. The iron content obtained from the EDS analysis closely agreed with both XPS elemental analysis and theoretical elemental composition. Table 1 summarizes the XPS elemental survey and micro-elemental analysis, along with the bonding type and oxidation states of each element.

Table 1. XPS survey analysis and elemental compositions and binding energies of Fe(III)-TA.

Elemental Transition Peak	Binding Energy (eV)	Chemical and Oxidation State	Elemental Analysis	
			Experimental	Theoretical
C 1s	284.1, 287.9	C-C (sp^3), O-C=O (sp^2)	45.79	46.28
Fe 2p 2p _{3/2} & 2p _{1/2}	701.9, 714.8, 729.9, 735.5, 723.6	Fe ⁺³ , Fe ⁺²	11.78 ^a /12.20 ^b	11.96
O 1s	530.2, 531.0, 532.4	Fe-O-C, C-O (sp^3), C=O (sp^2)	39.24 ^a	39.39
H	-	-	3.19	2.16

^a Obtained from XPS elemental survey analysis; ^b Obtained from EDS bulk elemental analysis.

Figure 2b–d represents the binding energy spectra for each element, confirming their oxidation states. The binding energy spectrum of Fe 2p, depicted in Figure 2b, showed that the oxidation state of Fe was +3 state from the corresponding two peaks, at 710.9 eV for Fe 2p_{3/2} and 725.9 eV for Fe 2p_{1/2}, confirming that the metal–phenolate bonds were indeed Fe(III)-O in $[\text{Fe}(-\text{CO})_6]$ metal oxide clusters. The accompanied two (less intense) satellite peaks at 714.8 and 735.5 of Fe 2p_{3/2} and Fe 2p_{1/2} were consistent with the presence of trivalent Fe, rather than di-valent Fe [25,26]. The presence of two well-resolved characteristic binding energy peaks for C 1s at 284.1 eV and 287.6 eV corresponded to C-C and O-C=O bonding, confirming the presence of tannic acid (Figure 2c). In the O 1s spectrum depicted in Figure 2d, Fe(III)-O bonding was confirmed from the peak at 530.2 eV, with a larger FWHM (4.44 eV), which further supported the oxygen chemical bonding state of O^{-2} , corresponding to the phenolate form. The binding energies of 531.0 eV and 532.4 eV, which corresponded to sp^3 C-O and sp^2 C=O, further supported the presence of glucose core units of the tannic acid. The bulk elemental distribution mapping obtained from the EDS analysis further supported the distribution of iron and the chemical composition of the microstructure (Figure 2e–h) and Figures S1 and S2 in the Supplementary Materials).

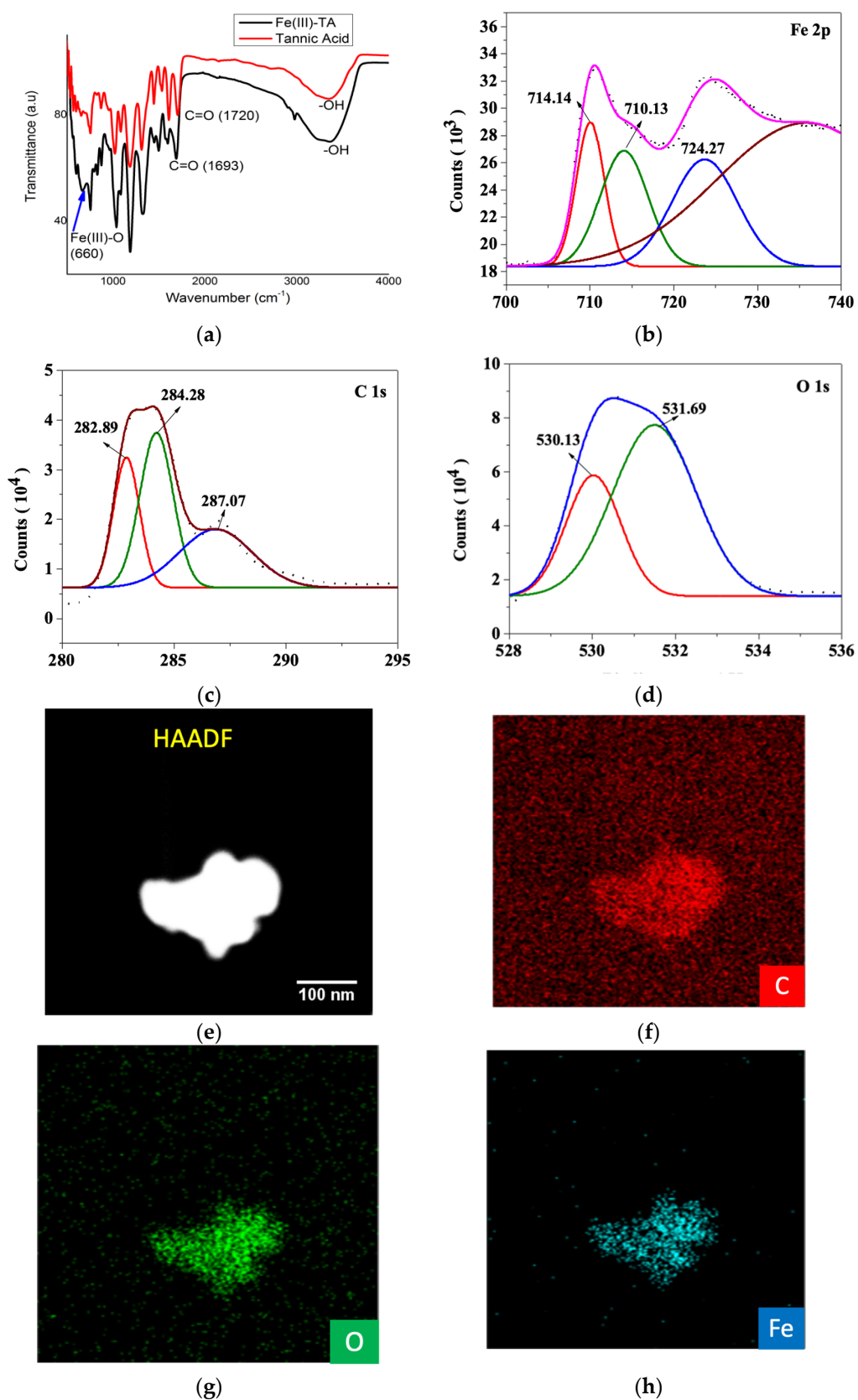


Figure 2. (a) FT-IR spectrum; Binding energy spectra of: (b) Fe 2p; (c) C 1s; (d) O 1s. STEM/EDS analysis images of: (e) HAADF-STEM and (f–h) elemental mapping for C, O, and Fe, respectively, for Fe(III)-TA.

3.3. Morphology and Surface Properties of Fe(III)-TA Microstructures

Morphologies of Fe(III)-TA microstructures were studied using scanning electron microscopy (SEM) and transmission electron microscopy (TEM), and are depicted in Figure 3. The SEM image (Figure 3a) of particles exhibited raspberry-like particles with aggregative clusters in a wide size distribution, ranging from an average size of ~50 nm in diameter for small particles to 100–300 nm in diameter for large particles and clusters. The TEM images of microstructures showed large cavities (10–25 nm in diameter, Figure 3b,c) along with nanopores <2 nm (in Figure 3d). The porosity, pore volume distribution and the N₂-adsorption Brunauer–Emmett–Teller Surface area (S_{BET}) were analyzed, utilizing Barret–Joyner–Halenda (BJH) and Brunauer–Emmett–Teller analyses. The BET adsorption-desorption linear isotherm and BJH desorption pore volume plots for BJH desorption cumulative pore volume and BJH desorption dV/dw are depicted in Figure S3 in the Supplementary Materials. Type II N₂ isotherm (Figure S3a in the Supplementary Materials), typical for microporous materials, was observed, with a S_{BET} of 70.47 m²/g and the micropore area of 7.04 m²/g. The BJH desorption average pore diameter was 27.2 nm, with a BJH desorption cumulative pore volume of 0.44 cm³/g (Figure S3b,c).

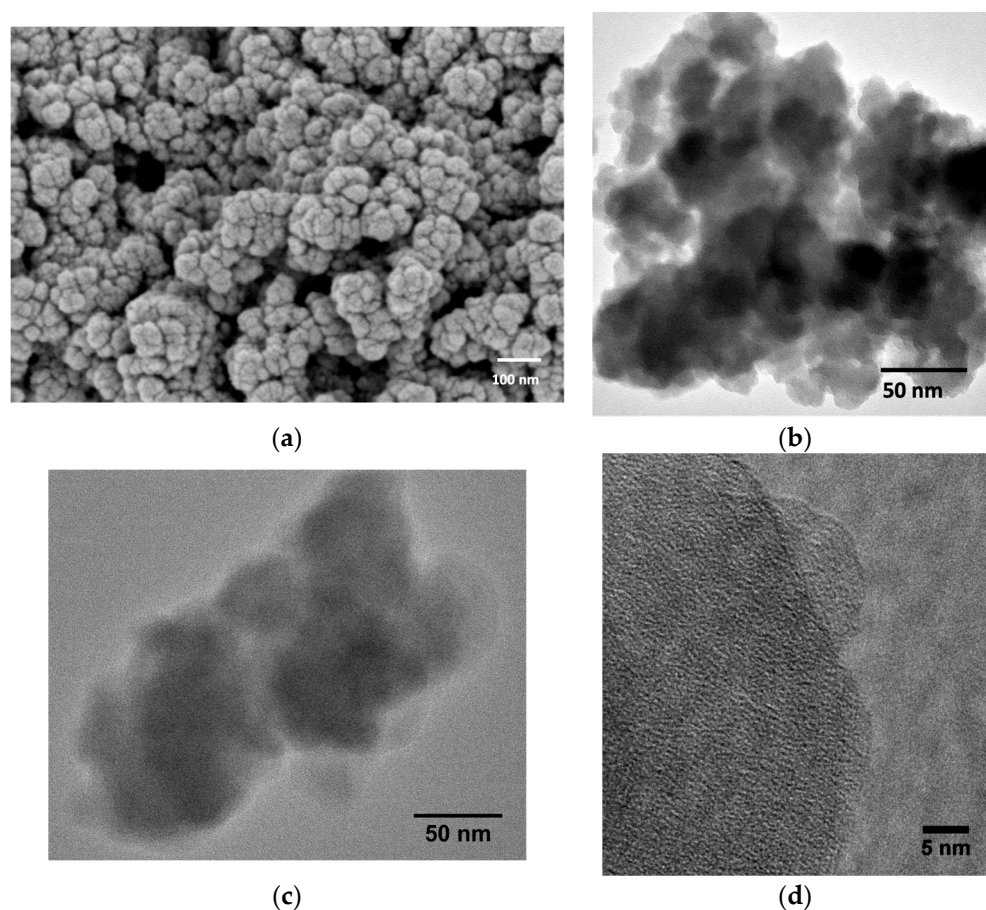


Figure 3. Morphology of Fe(III)-TA microstructure: (a) SEM image; (b–d) HR-TEM images representing pore distribution.

3.4. Thermal and Physiochemical Properties

The thermal stability of Fe(III)-TA, obtained from thermogravimetric analysis of the powder samples, exhibited three distinct weight losses at 180 °C, 350 °C, and 390 °C (Figure S4 in the Supplementary Materials). The initial weight loss of 13.7% at 180 °C could be ascribed to the decomposition of residual hydroxyl groups of peripheral pyrogallol units in the framework. The second and third weight losses at 350 °C and 390 °C demonstrated further decomposition of the pyrogallol and glucose units of the tannic acid, contributing to

the partial decomposition of organic content of the framework at 350 °C and the collapsing of the framework and complete decomposition of the organic content at 390 °C, respectively. The experimental weight loss of organic content was ~85%, comparable to the theoretical weight loss of organic content. There was no further weight loss after 390 °C, confirming the formation of carbonaceous products, which included iron oxide and char, contributing to the experimental weight loss of 14.98%. This weight loss was comparable to the theoretical weight loss for iron oxide and char yielded from organic content.

The pH-dependent surface properties and chemical stability of the microstructures in a colloidal solution of water and ethanol were evaluated by soaking the microstructures in a series of aqueous solutions of HCl and NaOH. The structure of microstructures remained intact over a large pH range: $2 < \text{pH} < 12$. The interfacial surface properties of the colloidal solution of Fe(III)-TA in water exhibited negative zeta potentials at all pH levels, reflecting negatively charged particles' surfaces. These contributed to the deprotonation of hydroxyl groups in peripheral pyrogallol units of tannic acid (Table 2 and Figure 4). The magnitude of the zeta potential gradually increased as the pH increased from 2 to 7, and colloids became very stable at $\text{pH} = 7$, exhibiting the highest zeta potential of -45.0 mV. This was evidence of the surface charge stabilization via electrostatic repulsions between particles, thereby avoiding flocculation and providing very good colloidal stability in water at $\text{pH} 7$ and above. In an aqueous solution of alcohol (70% ethanol), the colloidal solution of Fe(III)-TA exhibited amphoteric surface properties, with a positively charged particle surface at $\text{pH} < 4$ and a negatively charged surface at $\text{pH} > 4$.

Table 2. The physicochemical properties of a colloidal solution of microstructures.

pH of the Solution	Zeta Potential (eV)	
	in Water	in Ethanol
2	-2.0	8.0
4	-20.9	-4.5
6	-22.4	-19.0
7	-45.0	-23.8
10	-35.2	-8.4
12	-33.8	-10.1

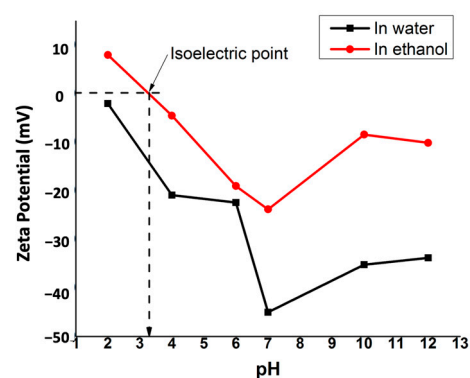


Figure 4. Zeta potential vs. pH of Fe(III)-TA colloids in water and ethanol.

3.5. Heavy Metal Adsorption Studies

To demonstrate the heavy metal sorption properties of our bio-based sorbent, Pb^{+2} ions adsorption efficiency was investigated using water samples with Pb^{+2} ion concentrations ranging from 20 ppm to 500 ppm. The equilibrium sorption capacity, with respect to the Pb^{+2} ion concentration, was calculated using Equation (1), and the respective equilibrium sorption curve and adsorption isotherm are depicted in Figure 5. The equilibrium sorption plot shown in Figure 5a exhibited excellent Pb^{+2} adsorption with 99% efficiency removing lead from water. The adsorption isotherm shown in Figure 5b, which was established using

the Langmuir model, exhibited a linear adsorption relationship, as stated by its linear form, Equation (2):

$$\frac{1}{q_e} = \frac{1}{q_m} + \frac{1}{q_m k_l C_e} \quad (2)$$

where q_e is the equilibrium sorption capacity, q_m is the maximum sorption capacity of the sorbent (saturation point), C_e is the concentration of heavy metal ion in solution at equilibrium [mg/L], and k_l is the Langmuir adsorption constant [L/mg].

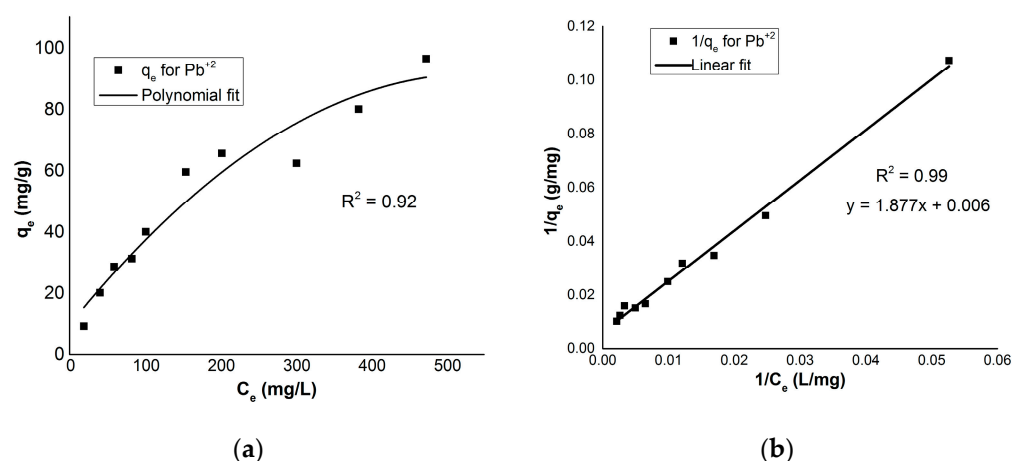


Figure 5. (a) Equilibrium sorption curve for Pb²⁺ and (b) adsorption isotherm curve, established for Pb²⁺ using Langmuir model.

The experimental sorption data fit very well to the Langmuir equation, with the highest average regression coefficients ($R^2 = 0.99$), denoting homogeneous adsorption and supporting the clear concept of monomolecular adsorption on homogenous charged surfaces [37]. The Langmuir adsorption constant (k_l), which was related to the apparent energy of sorption, was calculated to be 3.19×10^{-3} , and the maximum adsorption capacity (q_m) for Pb²⁺ was 166.66 mg/g. This initial study demonstrated that the porous microstructures of Fe(III)-TA showed energetically favorable adsorption of heavy metals. However, further investigation will be necessary to understand the heavy metal ion–sorbent interactions. Thus, future studies will focus on understanding the host–guest chemistry of heavy metal ion interactions with Fe(III)-TA by investigating the pH-dependent kinetic adsorption isotherms to reveal its adsorption mechanism.

4. Discussion

In summary, as the first bioinspired coordination polymer with a rigid framework synthesized from a polytopic natural polyphenol, the porous microstructure of the Fe(III)-TA coordination polymer demonstrated the use of biomass building blocks to construct environmentally benign, bioinspired porous microstructures using green synthesis, on a large scale, under ambient conditions in water. In a recent work, we reported the crystal structure (CCDC 2108217–2108218) of a dimer of iron(III)-tannate, confirming that Fe³⁺ coordinated to phenolate groups of each catechol unit by catenating up to four catechol units per one tannic acid molecule, supporting our empirical formula for the monomer unit of the coordination polymer framework [38]. In the dimer form, the coordination number for Fe³⁺ was six in its slightly disordered FeO₆ octahedral clusters, resulting in an overall charge-neutral coordination complex. In its dimer form, all three phenolate groups in four catechol units were presumed to be deprotonated, constructing metal–phenolate FeO₆ clusters, supporting the coordination geometry and stoichiometry of the metal–phenolate coordination nodes in the coordination polymer of iron(III)-tannate, constructing a robust framework. Microporosity, amphoteric surface properties, and colloidal stability in water at a wider range of pH, as well as Pb²⁺ adsorption, highlighted the potential of

microstructures of Fe(III)-TA and their potential utility as an amphoteric sorbent material for separation, extraction, and upcycling of toxic heavy metals, valuable minerals, and organic contaminants from water resources. For instance, the physiochemical surface properties of microstructures could provide greater insight into interfacial interactions with a variety of impurities present in water, enabling their use as sorbents for contaminant removal and separation from aqueous environments. Thus, our future work will focus on studying the absorption/desorption kinetics of microstructures for the purpose of removing a variety of heavy metal contaminants and other valuable minerals from a variety of water resources.

5. Conclusions

For the first time, we demonstrated a versatile green synthesis method to make porous iron-tannate microstructures (Fe(III)-TA) and their physiochemical properties. The Fe(III)-TA microstructures were synthesized by catenating the peripheral catechol groups in tannic acid with iron(II)acetate, using an environmentally friendly aqueous synthesis method under ambient conditions. This environmentally benign synthesis method facilitated a cost-effective, easy scale-up process. The structural and chemical compositions were analyzed, confirming the formation of an iron-tannate coordination polymer network with the empirical formula of $[\text{Fe}_4\text{C}_{76}\text{H}_{40}\text{O}_{46}]_n$. The surface area, porosity distribution, adsorption/desorption pore volume, and pH-responsive amphoteric behaviors of the iron-tannate microstructures were assessed, confirming their potential as a bioinspired porous material with amphoteric characteristics. Given the oxygen-rich functionality and highly porous robust framework, Fe(III)-TA microstructures have demonstrated the ability to extract Pb^{+2} present in water, with 99% extraction efficiency. The maximum adsorption capacity of the sorbent for Pb^{+2} was found to be 166.66 mg/g. The adsorption was energetically favorable and followed the linear form of the Langmuir isotherm model. Moreover, future studies on understanding and controlling the properties of highly porous, natural, polyphenol-based coordination polymer frameworks, including Fe(III)-TA, have great potential for the development of safe and innovative bio-based sorbents and will advance the host–guest chemistry of natural, amphoteric, polyphenol-based coordination polymer frameworks.

Supplementary Materials: The following supporting information can be downloaded at: <https://www.mdpi.com/article/10.3390/suschem3020013/s1>, Figure S1. EDS spectrum and elemental composition of Fe-TA microstructures. (Note: Pd and Au come from the sample coating for SEM imaging; Figure S2. EDS spectrum of Fe-TA microstructures obtained HR-TEM using STEMEDS capability; Figure S3. (a) N2-isotherm. (b) BHJ desorption cumulative pore volume distribution. (c) BHJ desorption dV/dw pore volume; Figure S4. TGA curve for Fe(III)-TA.

Author Contributions: The manuscript was written by H.R., with contributions from S.D. (65%), G.P. (15%), K.A. (15%), and O.A. (5%). All authors have read and agreed to the published version of the manuscript.

Funding: This research was funded by the NSF (Grant ECCS-1542174), DOD HBCU/MSI instrumentation award (Contract #: W911NF1910522), and USDA NIFA Equipment grant program (Award # NIFA EGP 2021-70410-35292). The APC was funded by Library, University of North Carolina at Greensboro.

Institutional Review Board Statement: No applicable.

Informed Consent Statement: No applicable.

Data Availability Statement: The Crystal structure of a dimer derivative of Fe(III)-TA microstructures reported herein can be accessed through Cambridge Crystallographic Data Center (CCDC) using the CCDC# 2108217–2108218. All other data relevant to the work is reported herein.

Acknowledgments: This work was performed at the Joint School of Nanoscience and Nanoengineering, a member of the South-eastern Nano-technology Infrastructure Corridor (SENIC) and National Nanotechnology Coordinated Infrastructure (NNCI), supported by the NSF (Grant ECCS-1542174). Authors also acknowledge the DOD HBCU/MSI instrumentation award (Contract #: W911NF1910522) used to acquire HR-TEM (JEOL 2100PLUS) with STEM/EDS capability and USDA NIFA equipment awarded to acquire Field-Emission SEM (JEOL IT800SEM) with EDS capability. Additionally, authors acknowledge Pravalika Butreddy for performing the EDS analysis.

Conflicts of Interest: The authors declare no conflict of interest.

References

1. Sarkar, R.; Pal, A.; Rakshit, A.; Saha, B. Properties and applications of amphoteric surfactant: A concise review. *J. Surfactants Deterg.* **2021**, *24*, 709–730. [[CrossRef](#)]
2. Eredyuk, V.; Alami, E.; Nydén, M.; Holmberg, K.; Peresyphkin, A.V.; Menger, F.M. Micellization and Adsorption Properties of Novel Zwitterionic Surfactants. *Langmuir* **2001**, *17*, 5160–5165. [[CrossRef](#)]
3. Li, Y.; Huang, C.; Yang, J.; Peng, J.; Jin, J.; Ma, H.; Chen, J. Multifunctionalized mesoporous silica as an efficient reversed-phase/anion exchange mixed-mode sorbent for solid-phase extraction of four acidic nonsteroidal anti-inflammatory drugs in environmental water samples. *J. Chromatogr. A* **2017**, *1527*, 10–17. [[CrossRef](#)] [[PubMed](#)]
4. Fontanals, N.; Borrull, F.; Marcé, R.M. Mixed-mode ion-exchange polymeric sorbents in environmental analysis. *J. Chromatogr. A* **2020**, *1609*, 460531. [[CrossRef](#)]
5. Andrade-Eiroa, A.; Canle, M.; Leroy-Cancellieri, V.; Cerdà, V. Solid-phase extraction of organic compounds: A critical review. Part II. *TrAC Trends Anal. Chem.* **2016**, *80*, 655–667. [[CrossRef](#)]
6. Madikizela, L.M.; Ncube, S.; Chimuka, L. Recent developments in selective materials for solid phase extraction. *Chromatographia* **2019**, *82*, 1171–1189. [[CrossRef](#)]
7. Houk, R.J.T.; Jacobs, B.W.; Gabaly, F.E.; Chang, N.N.; Talin, A.A.; Graham, D.D.; House, S.D.; Robertson, I.M.; Allendorf, M.D. Silver Cluster Formation, Dynamics, and Chemistry in Metal–Organic Frameworks. *Nano Lett.* **2009**, *9*, 3413–3418. [[CrossRef](#)]
8. Burtch, N.C.; Jasnaja, H.; Walton, K.S. Water stability and adsorption in metal–organic frameworks. *Chem. Rev.* **2014**, *114*, 10575–10612. [[CrossRef](#)]
9. Auriemma, M.; Piscitelli, A.; Pasquino, R.; Cerruti, P.; Malinconico, M.; Grizzuti, N. Blending poly (3-hydroxybutyrate) with tannic acid: Influence of a polyphenolic natural additive on the rheological and thermal behavior. *Eur. Polym. J.* **2015**, *63*, 123–131. [[CrossRef](#)]
10. Makris, D.P.; Boskou, G.; Andrikopoulos, N.K. Polyphenolic content and in vitro antioxidant characteristics of wine industry and other agri-food solid waste extracts. *J. Food Compos. Anal.* **2007**, *20*, 125–132. [[CrossRef](#)]
11. Shutava, T.; Prouty, M.; Kommireddy, D.; Lvov, Y. pH Responsive Decomposable Layer-by-Layer Nanofilms and Capsules on the Basis of Tannic Acid. *Macromolecules* **2005**, *38*, 2850–2858. [[CrossRef](#)]
12. Erel-Unal, I.; Sukhishvili, S.A. Hydrogen-Bonded Multilayers of a Neutral Polymer and a Polyphenol. *Macromolecules* **2008**, *41*, 3962–3970. [[CrossRef](#)]
13. Fan, H.; Wang, L.; Feng, X.; Bu, Y.; Wu, D.; Jin, Z. Supramolecular Hydrogel Formation Based on Tannic Acid. *Macromolecules* **2017**, *50*, 666–676. [[CrossRef](#)]
14. Ejima, H.; Richardson, J.J.; Liang, K.; Best, J.P.; van Koeverden, M.P.; Such, G.K.; Cui, J.; Caruso, F. One-step assembly of coordination complexes for versatile film and particle engineering. *Science* **2013**, *341*, 154–157. [[CrossRef](#)]
15. Li, W.; Bing, W.; Huang, S.; Ren, J.; Qu, X. Mussel Byssus-Like Reversible Metal-Chelated Supramolecular Complex Used for Dynamic Cellular Surface Engineering and Imaging. *Adv. Funct. Mater.* **2015**, *25*, 3775–3784. [[CrossRef](#)]
16. Rahim, M.A.; Kempe, K.; Müllner, M.; Ejima, H.; Ju, Y.; van Koeverden, P.M.; Suma, T.; Braunger, J.A.; Leeming, M.G.; Abrahams, B.F.; et al. Surface-Confined Amorphous Films from Metal-Coordinated Simple Phenolic Ligands. *Chem. Mater.* **2015**, *27*, 5825–5832. [[CrossRef](#)]
17. Rahim, M.A.; Björnmalm, M.; Suma, T.; Faria, M.; Ju, Y.; Kempe, K.; Müllner, M.; Ejima, H.; Stickland, A.D.; Caruso, F. Metal–Phenolic Supramolecular Gelation. *Angew. Chem. Int. Ed.* **2016**, *55*, 13803–13807. [[CrossRef](#)]
18. Rahim, M.A.; Björnmalm, M.; Bertleff-Zieschang, N.; Besford, Q.; Mettu, S.; Suma, T.; Faria, M.; Caruso, F. Rust-Mediated Continuous Assembly of Metal–Phenolic Networks. *Adv. Mater.* **2017**, *29*, 1606717. [[CrossRef](#)]
19. Erwin, W.R.; Zarick, H.F.; Talbert, E.M.; Bardhan, R. Light trapping in mesoporous solar cells with plasmonic nanostructures. *Energy Environ. Sci.* **2016**, *9*, 1577–1601. [[CrossRef](#)]
20. Chen, Y.; Shi, J. Chemistry of Mesoporous Organosilica in Nanotechnology: Molecularly Organic–Inorganic Hybridization into Frameworks. *Adv. Mater.* **2016**, *28*, 3235–3272. [[CrossRef](#)]
21. Gao, Z.; Zharov, I. Large Pore Mesoporous Silica Nanoparticles by Templating with a Nonsurfactant Molecule, Tannic Acid. *Chem. Mater.* **2014**, *26*, 2030–2037. [[CrossRef](#)]
22. Jiang, Y.; Sun, W.; Zhou, L.; Ma, L.; He, Y.; Gao, J. Improved Performance of Lipase Immobilized on Tannic Acid-Templated Mesoporous Silica Nanoparticles. *Appl. Biochem. Biotechnol.* **2016**, *179*, 1155–1169. [[CrossRef](#)] [[PubMed](#)]

23. Gao, J.; Lei, H.; Han, Z.; Shi, Q.; Chen, Y.; Jiang, Y. Dopamine functionalized tannic-acid-templated mesoporous silica nanoparticles as a new sorbent for the efficient removal of Cu²⁺ from aqueous solution. *Sci. Rep.* **2017**, *7*, 45215. [[CrossRef](#)] [[PubMed](#)]
24. Park, J.H.; Choi, S.; Moon, H.C.; Seo, H.; Kim, J.Y.; Hong, S.-P.; Lee, B.S.; Kang, E.; Lee, J.; Ryu, D.H.; et al. Antimicrobial spray nanocoating of supramolecular Fe(III)-tannic acid metal-organic coordination complex: Applications to shoe insoles and fruits. *Sci. Rep.* **2017**, *7*, 6980. [[CrossRef](#)]
25. Saowalak, K.; Titipun, T.; Somchai, T.; Chalermchai, P. Iron(III)-Tannic Molecular Nanoparticles Enhance Autophagy effect and T1 MRI Contrast in Liver Cell Lines. *Sci. Rep.* **2018**, *8*, 6647. [[CrossRef](#)]
26. Krungchanuchat, S.; Thongtem, T.; Thongtem, S.; Pilapong, C. Characterization and cellular studies of molecular nanoparticle of iron (III)-tannic complexes; toward a low cost magnetic resonance imaging agent. *Biointerphases* **2017**, *12*, 021005. [[CrossRef](#)]
27. Kim, H.J.; Kim, D.-G.; Yoon, H.; Choi, Y.-S.; Yoon, J.; Lee, J.-C. Polyphenol/FeIII Complex Coated Membranes Having Multifunctional Properties Prepared by a One-Step Fast Assembly. *Adv. Mater. Interfaces* **2015**, *2*, 1500298. [[CrossRef](#)]
28. Yang, L.; Han, L.; Ren, J.; Wei, H.; Jia, L. Coating process and stability of metal-polyphenol film. *Colloids Surf. A Physicochem. Eng. Asp.* **2015**, *484*, 197–205. [[CrossRef](#)]
29. Rahim, M.A.; Ejima, H.; Cho, K.L.; Kempe, K.; Müllner, M.; Best, J.P.; Caruso, F. Coordination-Driven Multistep Assembly of Metal-Polyphenol Films and Capsules. *Chem. Mater.* **2014**, *26*, 1645–1653. [[CrossRef](#)]
30. Nguyen, N.T.T.; Furukawa, H.; Gándara, F.; Trickett, C.A.; Jeong, H.M.; Cordova, K.E.; Yaghi, O.M. Three-Dimensional Metal-Catecholate Frameworks and Their Ultrahigh Proton Conductivity. *J. Am. Chem. Soc.* **2015**, *137*, 15394–15397. [[CrossRef](#)]
31. Yang, S.J.; Antonietti, M.; Fechler, N. Self-Assembly of Metal Phenolic Mesocrystals and Morphosynthetic Transformation toward Hierarchically Porous Carbons. *J. Am. Chem. Soc.* **2015**, *137*, 8269–8273. [[CrossRef](#)] [[PubMed](#)]
32. Zhang, P.; Li, H.; Veith, G.M.; Dai, S. Soluble Porous Coordination Polymers by Mechanochemistry: From Metal-Containing Films/Membranes to Active Catalysts for Aerobic Oxidation. *Adv. Mater.* **2015**, *27*, 234–239. [[CrossRef](#)] [[PubMed](#)]
33. Wei, J.; Liang, Y.; Hu, Y.; Kong, B.; Zhang, J.; Gu, Q.; Tong, Y.; Wang, X.; Jiang, S.P.; Wang, H. Hydrothermal Synthesis of Metal-Polyphenol Coordination Crystals and Their Derived Metal/N-doped Carbon Composites for Oxygen Electrocatalysis. *Angew. Chem.* **2016**, *128*, 12658–12662. [[CrossRef](#)]
34. Aktar, J.; Ray, M. Iron-polyphenol nanocluster removes fluoride and methylene blue dye from water and promotes plant growth. *SSRN* **2022**, *32*. [[CrossRef](#)]
35. Elmorsi, T.M. Synthesis of Nano-Titanium Tannate as an Adsorbent for Crystal Violet Dye, Kinetic and Equilibrium Isotherm Studies. *J. Environ. Prot.* **2015**, *6*, 1454–1471. [[CrossRef](#)]
36. Zhang, R.; Li, L.; Liu, J. Synthesis and characterization of ferric tannate as a novel porous adsorptive-catalyst for nitrogen removal from wastewater. *RSC Adv.* **2015**, *5*, 40785–40791. [[CrossRef](#)]
37. Chen, J.P. *Decontamination of Heavy Metals: Processes, Mechanisms, and Applications*; CRC Press: Boca Raton, FL, USA, 2012.
38. Rathnayake, H. *CCDC 2108217: Experimental Crystal Structure Determination*; The Cambridge Crystallographic Data Centre (CCDC): Cambridge, UK, 2021.